Biological Cybernetics (2019) 113:105–120
https://doi.org/10.1007/s00422-018-0781-y

Biological Cybernetics

ORIGINAL ARTICLE

Cardiovascular regulation in response to multiple hemorrhages: analysis and parameter estimation

Maria-Veronica Ciocanel[1] · Steffen S. Docken[2] · Rebecca E. Gasper[3] · Caron Dean[4] · Brian E. Carlson[5] · Mette S. Olufsen[6]

Received: 5 February 2018 / Accepted: 2 September 2018 / Published online: 12 September 2018

Abstract

Mathematical models can provide useful insights explaining behavior observed in experimental data; however, rigorous analysis is needed to select a subset of model parameters that can be informed by available data. Here we present a method to estimate an identifiable set of parameters based on baseline left ventricular pressure and volume time series data. From this identifiable subset, we then select, based on current understanding of cardiovascular control, parameters that vary in time in response to blood withdrawal, and estimate these parameters over a series of blood withdrawals. These time-varying parameters are first estimated using piecewise linear splines minimizing the mean squared error between measured and computed left ventricular pressure and volume data over four consecutive blood withdrawals. As a final step, the trends in these splines are fit with empirical functional expressions selected to describe cardiovascular regulation during blood withdrawal. Our analysis at baseline found parameters representing timing of cardiac contraction, systemic vascular resistance, and cardiac contractility to be identifiable. Of these parameters, vascular resistance and cardiac contractility were varied in time. Data used for this study were measured in a control Sprague-Dawley rat. To our knowledge, this is the first study to analyze the response to multiple blood withdrawals both experimentally and theoretically, as most previous studies focus on analyzing the response to one large blood withdrawal. Results show that during each blood withdrawal both systemic vascular resistance and contractility decrease acutely and partially recover, and they decrease chronically across the series of blood withdrawals.

Keywords Blood withdrawal · Cardiovascular regulation · Mathematical modeling · Parameter estimation · Left ventricular volume · Left ventricular pressure

1 Introduction

As more high fidelity physiological experimental data become available, there is a greater need for mechanistic mathematical models of the system being investigated to aid in understanding the experimental observations. An increasing amount of experimental data consists of time series data that

Communicated by Peter J. Thomas.

This article belongs to the Special Issue on *Control Theory in Biology and Medicine.* It derived from a workshop at the Mathematical Biosciences Institute, Ohio State University, Columbus, OH, USA.

Electronic supplementary material The online version of this article (https://doi.org/10.1007/s00422-018-0781-y) contains supplementary material, which is available to authorized users.

✉ Mette S. Olufsen
msolufse@ncsu.edu

Maria-Veronica Ciocanel
ciocanel.1@mbi.osu.edu

Steffen S. Docken
ssdocken@math.ucdavis.edu

Rebecca E. Gasper
rebeccagasper@creighton.edu

Caron Dean
cdean@mcw.edu

Brian E. Carlson
bcarl@umich.edu

1 The Ohio State University, Columbus, USA

2 University of California, Davis, Davis, USA

3 Creighton University, Omaha, USA

4 Medical College of Wisconsin, Milwaukee, USA

5 University of Michigan, Ann Arbor, USA

6 North Carolina State University, Raleigh, USA

track one or more variables in time either acutely or chronically. In addition, mathematical models used to replicate these datasets are found at all scales: multiple organ system (e.g., the cardiovascular system), organ, cellular and subcellular [2,16,31,35]. Once a physiologically based model is chosen, the question is how to ensure that a proper set of model parameters is selected to reproduce the experimental data. Much work has been done to develop methods for selecting parameters that can be informed by the data. Algorithms and procedures for parameter identifiability have been developed based on the Fisher information matrix [1,7], profile likelihoods [28], analytical approaches [32], and many other techniques reviewed in Chis et al. [6]. While these methods apply to a wide range of models and data, no single approach generalizes to all experimental and modeling contexts [6]. These methods have been used for the study of cardiovascular models [21,23,25] and here they are adapted for analyzing the cardiovascular response to successive blood withdrawals. In this study, we develop a robust workflow to analyze the dynamic response to blood withdrawal. The workflow starts by using subject-specific information to inform a baseline model predicting blood pressure and heart rate dynamics at homeostasis (before blood withdrawal). A subset of identifiable parameters are selected and estimated to fit baseline data. From these, we select parameters regulated by the cardiovascular system and show how they can represent experimental data under perturbation conditions (blood withdrawal).

The experimental data used to illustrate this analytical approach is from simultaneous measurement of rat left ventricular pressure and volume at baseline and then during a series of blood withdrawals, performed to observe how the cardiovascular function changes during hemorrhage. Autonomic regulation of the cardiovascular system drives changes in cardiovascular function by responding to changes in mean arterial pressure. It controls heart rate, cardiac contractility, and total peripheral resistance in an effort to restore blood pressure and tissue perfusion [30] and consists of an acute component (on the scale of seconds) and a longer timescale component (on the scale of minutes to hours) [3]. Many studies have observed autonomic regulation of the cardiovascular system in response to a single blood withdrawal in experimental animal studies [4,14]. Other studies have performed multiple blood withdrawals in animals in an effort to identify the maximal amount and interval between blood withdrawals to minimize the autonomic regulatory response when observing other cardiovascular phenomena [29]. To our knowledge, no studies have been performed to understand the variation in the autonomic regulatory response of the cardiovascular system across multiple blood withdrawals.

As noted, our workflow consists of two major steps: (1) Prediction of baseline dynamics (before blood withdrawal); and (2) Modeling the response to blood withdrawals.

To study baseline dynamics, we use a simple cardiovascular model adapted from Williams et al. [34]. The model by Williams et al. was parametrized for humans and set up to predict arterial blood pressure. The model proposed here uses heart rate as an input to predict blood pressure, flow, and volume in five compartments representing the left ventricle, large and small arteries and veins. We parametrize this model to a mouse system and analyze predictions of left ventricular pressure and volume. Using covariance analysis [21,34], we identify a subset of five parameters that can be estimated to fit the baseline experimental data (left ventricular pressure and volume).

To study the response to successive blood withdrawals, we select three parameters from the subset estimated at baseline and allow them to vary in time. These parameters are known to be modulated by the cardiovascular control system. Similar to the study of head-up tilt in humans by Williams et al. [34], the time-varying parameters are represented by piecewise linear splines with estimated spline nodes minimizing the least squares error between model predictions and experimental data. In addition, our work goes beyond Williams et al. [34] by setting up functional representations of these splines to capture the time-varying characteristics as a function of aortic blood pressure and left ventricular volume, quantities that are known to be inputs to the autonomic and passive control of the cardiovascular system.

2 Methods

This study includes a series of blood withdrawal experiments with continuous measurements of left ventricular blood pressure and voltage (converted to volume) analyzed using a five-compartment model. To characterize the autonomic and passive cardiovascular control in response to hemorrhage, we use time-varying parameters represented by piecewise linear splines and dynamic models. We use sensitivity analysis and covariance-based subset selection methodology to determine a subset of identifiable parameters and use nonlinear optimization to estimate the identifiable parameters minimizing the least squares error between model predictions and data.

2.1 Experimental methods

In this work, we use data from one male Sprague-Dawley rat to study changes in cardiovascular function in response to multiple blood withdrawals. The weight of the rat and additional experimental parameters are summarized in Table 1. In the experiment, the animal is anesthetized with sodium phenobarbital and catheters are placed in the femoral artery and vein for blood withdrawal and the administration of anesthetics. A pressure-volume conduction catheter (Millar SPR-869, 2F tip with four electrodes and 6 mm spacing) is inserted

Table 1 Experimental measurements

Rat weight (g)	339			
Estimated blood volume (ml)	19.323			
	BW1	BW2	BW3	BW4
Amount withdrawn (ml)	1	1, 1	1, 1	1
Duration of withdrawal (s)	19	26, 15	17, 28	30
Length of cardiac cycle (s)	0.27	0.27	0.29	0.32
Mean BP (mmHg)	50.4	39.0	24.6	11.5

The two times listed for BW2 and BW3 correspond to the duration of consecutive withdrawals of 1 ml each
BW blood withdrawal, *BP* blood pressure

through the right carotid artery into the left ventricle to simultaneously obtain pressure and voltage measurements. The pressure data are used directly in the model analysis, while the voltage data are converted to volume as described below. The experimental protocol consists of four blood withdrawals separated by a period of rest lasting at least 2 min, included to ensure that the cardiovascular control system is in steady state at the onset of each blood withdrawal. We refer to each new equilibrium/rest state as "baseline" while the period over which blood is withdrawn and the animal recovers is referred to as "blood withdrawal." The data are shown in Fig. 1 in its entirety. In this study, we extract four time intervals representing 90–180 s of data each (marked with dark gray on the figure) including a baseline phase (its endpoint is marked with a blue asterisk) and a blood withdrawal phase. The baseline data, before the first blood withdrawal, are analyzed by Marquis et al. [21], but the complete signal with four blood withdrawals has not been published previously.

2.1.1 Calibration

To obtain volume data, it is necessary to convert voltage measurements to volume. This is typically done using cuvette calibrations performed by withdrawing blood, filling cuvettes of different volume and taking conduction catheter readings in each cuvette. This calibration is usually done at the end of the actual experiment. For this study, the cuvette readings taken after the blood withdrawal sequence could not be used for predicting volumes at the baseline time points, likely since the blood chemistry and hence conductivity change over the time course of the blood withdrawals.

To overcome this problem, we developed a novel methodology combining information from cuvette measurements with literature data. To do so, we assume that at baseline prior to the first blood withdrawal, the left ventricular end diastolic and end systolic volumes scale with animal weight, as previously suggested [18]. We use literature values from MRI-based volume measurement studies (adopted as the gold standard for ventricular volume determination) to convert these baseline voltage measurements from the conduction catheter into baseline ventricular volumes. Trends

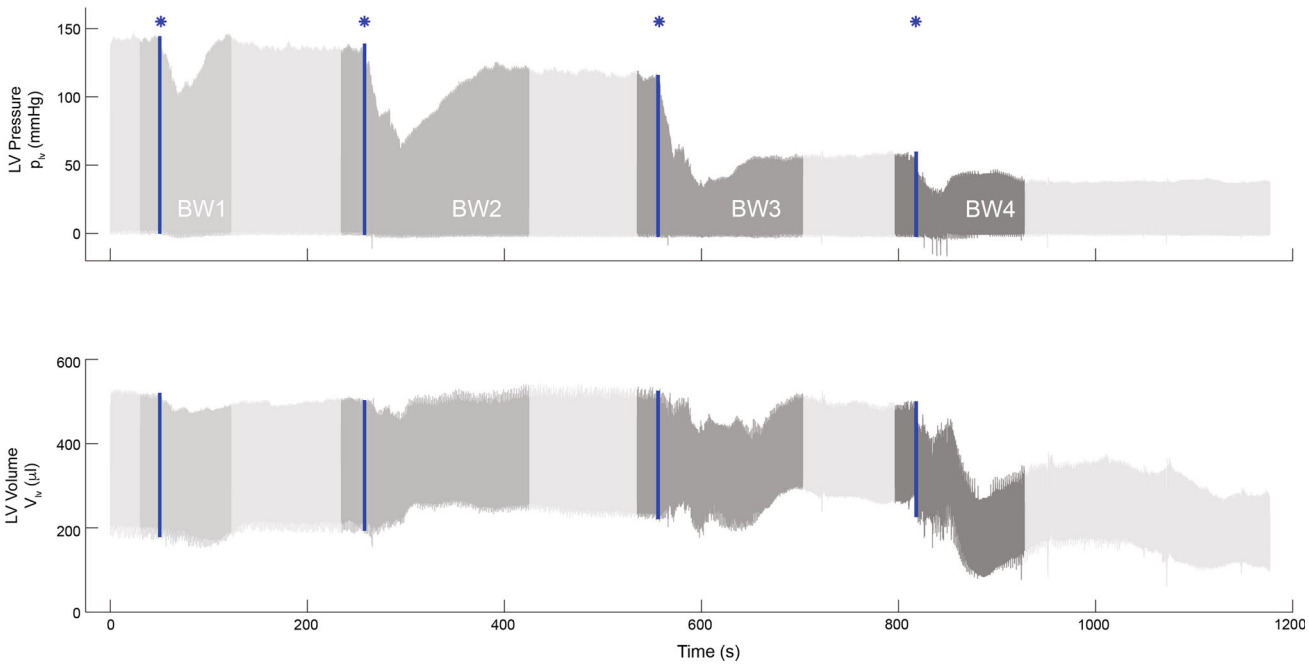

Fig. 1 Pressure and volume (converted from voltage) signal for the complete blood withdrawal experiment. Four blood withdrawal segments (BW1–BW4 dark gray) are extracted for analysis including a short baseline phase and a blood withdrawal phase. The end of the baseline phase is marked by a vertical line with a asterisk on top

for the left ventricular end diastolic and stroke volumes as a function of body weight from control animals in thirteen MRI-based studies are used to set the baseline calibration. This relationship between ventricular volume and stroke volume to weight is depicted in the Electronic Supplementary Material. The cuvette calibration of voltage to volume is then used (where the calibration is valid) to convert voltage to volume during the steady state after the final blood withdrawal. These two voltage-to-volume calibration points at the beginning and end of the experiment are then used to scale volume for the entire series of blood withdrawals.

2.2 Mathematical model

Blood flow and pressure are predicted using a five-compartment model (see Fig. 2 and Table 2) consisting of large and small arteries and veins as well as a beating heart. Equations relating pressure, flow, and volume are derived assuming that the dynamics follow an electrical circuit analogy with pressure p (mmHg) analogous to voltage, flow q (μl/s) analogous to current, and volume V (μl) analogous to charge. Using these assumptions, for each compartment, conservation of volume gives

$$\frac{\mathrm{d}V_i}{\mathrm{d}t} = q_{i-1} - q_i, \tag{1}$$

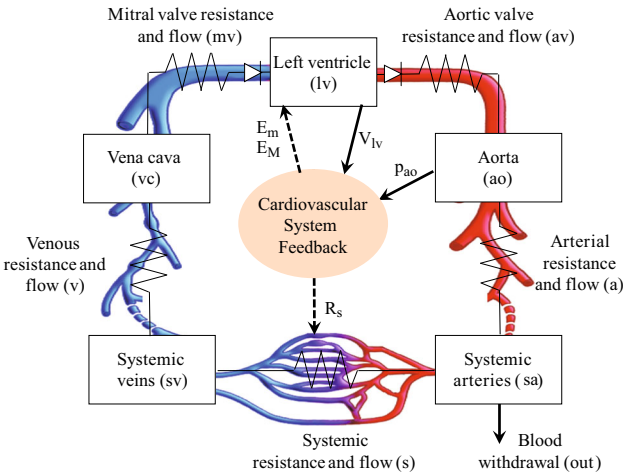

Fig. 2 Schematic of the compartment model, showing the five compartments and the cardiovascular controls. The model includes the systemic circulation represented by two arterial and two venous compartments coupled by a left ventricle representing the beating heart. Since our model does not include flow in the pulmonary circulation, the large veins directly feed into the left ventricle. All compartments are compliant, and compartments are separated by resistors scaled to ensure appropriate pressure distribution within the system. To model the cardiovascular control, systemic resistance R_s and cardiac contractility parameters E_M, E_m are predicted as functions of aortic pressure and ventricular volume. Note: the heart rate is controlled as well, but in this study it is included as a model input

Table 2 List of model components and notation

Compartment	Pressure (mmHg)	Volume (μl)	Elastance (mmHg/μl)
Aorta (ao)	$p_{\mathrm{ao}}^{\mathrm{b}}$	V_{ao}	E_{ao}
Systemic arteries (sa)	p_{sa}	V_{sa}	E_{sa}
Systemic veins (sv)	p_{sv}	V_{sv}	E_{sv}
Vena cava (vc)	p_{vc}	V_{vc}	E_{vc}
Left ventricle (lv)	p_{lv}	$V_{\mathrm{lv}}^{\mathrm{b}}$	$E_{\mathrm{lv}}^{\mathrm{a}}$
Between compartments		**Flow (μl/s)**	**Resistance (mmHgs/μl)**
lv → ao		q_{av}	R_{av}
ao → sa		q_{a}	R_{a}
sa → sv		q_{s}	$R_{\mathrm{s}}^{\mathrm{a}}$
sv → vc		q_{v}	R_{v}
vc → lv		q_{mv}	R_{mv}

[a]Parameters E_{lv} and R_{s} are functions of autonomic response. [b]Variables p_{ao} and V_{lv} are control inputs
av aortic valve, a arterial, s systemic, v venous, mv mitral valve

where i denotes compartment $i \in \{\mathrm{ao}, \mathrm{sa}, \mathrm{sv}, \mathrm{vc}, \mathrm{lv}\}$ (see Fig. 2 and Table 2), and q_i represents the flow out of compartment i (i.e., change in volume is the flow in minus the flow out). For each compartment, the volume can be separated into a stressed volume (the part of the volume pumped around the circulation) and an unstressed volume, i.e.,

$$V_{i,\mathrm{tot}} = V_i + V_{i,0},$$

where $V_{i,0}$ denoting the unstressed volume is assumed constant. The subscript 0 refers to unstressed volume throughout the text.

Flow q (between compartments) and pressure p (inside compartments) are related to resistance R via Ohm's law

$$q_i = \frac{p_i - p_{i+1}}{R_i}, \tag{2}$$

where subscript i refers to the flow and pressure in question (see Fig. 2). Finally, pressure and volume are related to elastance E using

$$V_i - V_{i,0} = \frac{p_i - p_{i,0}}{E_i}, \tag{3}$$

where $p_{i,0}$ denotes the associated unstressed pressure in compartment i. For this study, we assume that $p_{i,0} = 0$.

To model the beating heart, for each cardiac cycle of period T ($T = 1/\mathrm{HR}$, the inverse of heart rate, input to the model), we use a time-varying model to compute left ventricular elastance $E_{\mathrm{lv}}(t)$. Equivalent to Eq. (3), the pressure in the left ventricle is given by

$$p_{\mathrm{lv}} = E_{\mathrm{lv}}(t)(V_{\mathrm{lv}} - V_{\mathrm{lv},0}),$$
$$E_{\mathrm{lv}}(t) = \begin{cases} \frac{E_{\mathrm{M}} - E_{\mathrm{m}}}{2}\left(1 - \cos\left(\frac{\pi t}{T_{\mathrm{s}}}\right)\right) + E_{\mathrm{m}}, & t < T_{\mathrm{s}} \\ \frac{E_{\mathrm{M}} - E_{\mathrm{m}}}{2}\left(1 + \cos\left(\frac{\pi(t - T_{\mathrm{s}})}{T_r - T_{\mathrm{s}}}\right)\right) + E_{\mathrm{m}}, & T_{\mathrm{s}} \le t < T_r \\ E_{\mathrm{m}}, & T_r \le t < T \end{cases} \quad (4)$$

where $T_{\mathrm{s}} = \alpha_{\mathrm{s}} T$ denotes the time in the cardiac cycle to maximal contractility and $T_r = \alpha_r T$ denotes the combined time in the cardiac cycle for the contractility to rise and return to its minimum in diastole [10].

Finally, to ensure proper function of the valves we let

$$q_{\mathrm{valve}} = \begin{cases} \frac{p_i - p_{i+1}}{R_{\mathrm{valve}}}, & p_i > p_{i+1} \ \text{(open valve)} \\ 0, & \text{otherwise.} \end{cases},$$

where q_{valve} is the flow through the aortic and mitral valves $q_{\mathrm{valve}} \in \{q_{\mathrm{av}}, q_{\mathrm{mv}}\}$. p_i denotes the pressure before the valve and p_{i+1} is the pressure after the valve. Here we assume that the valves can be modeled as diodes, i.e., that they are either open or closed.

The dynamics of the system are obtained by solving a system of five linear differential equations of the form (1), one for each compartment (full list of equations are given in the "Appendix"). Equations are solved numerically using MATLAB's built-in differential equations solver `ode15s`.

2.3 Nominal parameter values

Similar to the study by Marquis et al. [21], nominal parameter values for baseline simulations preceding each blood withdrawal (given in Table 3) are calculated using a combination of literature values and information extracted from data. To approximate parameters based on data, two steps are needed: first we approximate average baseline values for volume, pressure, and flow, then we solve model equations to extract nominal parameter values.

2.3.1 Volume

The total blood volume is estimated by $V_{\mathrm{tot}} = 57W\,\mu\mathrm{l}$ (where W is the rat weight in grams [33]). This volume is split into a stressed and an unstressed component using results from mammalian studies suggesting that approximately 30% of the total blood volume is stressed [12,33,36]. Of the 30%, we assume that 25% of the volume resides in arterial compartments and 75% resides in venous compartments, with systemic arteries and veins containing 90% of the arterial and venous volume [17,19].

2.3.2 Pressure

Initial pressures are estimated from data, assuming the systolic (maximal) aortic pressure is 99% of the maximum ventricular pressure (measured), and that the systolic systemic arterial pressure is 99% of the systolic aortic pressure. Similarly, on the venous side, the mean pressure in vena cava is assumed to be 10% higher than minimum left ventricular pressure, and the systemic venous pressure is assumed to be 10% higher than the vena cava pressure [21]. On the arterial side, we assume that the arterial pulse pressure is 30 mmHg and that mean arterial pressure ($p_{i,\mathrm{mean}}$) can be predicted as

$$p_{i,\mathrm{mean}} = \frac{2}{3}\, p_{i,\mathrm{dia}} + \frac{1}{3}\, p_{i,\mathrm{sys}} \quad (5)$$

Table 3 Table of nominal parameter values for baseline simulations preceding each blood withdrawal

Param	Value	Param	Value
V_{ao}	0.025 V_{tot}	p_{ao}	0.99 avg($p_{\mathrm{lv,sys}}$)
		$p_{\mathrm{ao,mean}}$	Equation (5), $i = ao$
V_{sa}	0.2 V_{tot}	p_{sa}	0.99 p_{ao}
		$p_{\mathrm{sa,mean}}$	Equation (5), $i = sa$
V_{vc}	0.075 V_{tot}	p_{vc}	1.1 avg($p_{\mathrm{lv,dia}}$)
V_{sv}	0.7 V_{tot}	p_{sv}	1.1 p_{vc}
$V_{\mathrm{lv},0}$	0.2 avg($V_{\mathrm{lv,min}}$)		
α_{s}	0.25	E_{m}	Equation (6)
α_r	0.6	E_{M}	Equation (7)
R_{a}	$(p_{\mathrm{ao,mean}} - p_{\mathrm{sa,mean}})/\mathrm{CO}$	E_{ao}	$p_{\mathrm{ao}} V_{\mathrm{ao}}$
R_{s}	$(p_{\mathrm{sa,mean}} - p_{\mathrm{sv}})/\mathrm{CO}$	E_{sa}	$p_{\mathrm{sa}} V_{\mathrm{sa}}$
R_{v}	$(p_{\mathrm{sv}} - p_{\mathrm{vc}})/\mathrm{CO}$	E_{vc}	$p_{\mathrm{vc}} V_{\mathrm{vc}}$
R_{av}	$\mathrm{avg}((p_{\mathrm{lv,max}}) - p_{\mathrm{ao}})/\mathrm{CO}$	C_{sv}	$p_{\mathrm{sv}} V_{\mathrm{sv}}$
R_{mv}	$p_{\mathrm{vc}} - \mathrm{avg}(p_{\mathrm{lv,min}})/\mathrm{CO}$		

V_{tot} total stressed volume (0.3 of total blood volume); CO cardiac output; (min, max): minimum and maximum pressure or volume averaged over each period

where i = ao for aortic compartment and sa for systemic compartment (see Fig. 2 and Table 2), subscripts "dia" and "sys" refer to diastolic (minimum) and systolic (maximum) values, respectively [3].

2.3.3 Flow

The flow through the system (cardiac output, or CO) is extracted from measurements of left ventricular volume:

$$\mathrm{CO} = \mathrm{HR} \cdot V_{\mathrm{stroke}},$$

where HR is the mean heart rate and

$$V_{\mathrm{stroke}} = V_{\mathrm{lv,max}} - V_{\mathrm{lv,min}}$$

is the mean stroke volume.

2.3.4 Parameter values

Model parameters include resistances, elastances, and heart parameters:

$$\theta \in \{R_{\mathrm{a}}, R_{\mathrm{s}}, R_{\mathrm{v}}, R_{\mathrm{av}}, R_{\mathrm{mv}}, E_{\mathrm{ao}}, E_{\mathrm{sa}}, E_{\mathrm{sv}}, E_{\mathrm{vc}}, \alpha_{\mathrm{s}}, \alpha_r, E_{\mathrm{m}}, E_{\mathrm{M}}\}.$$

Arterial and venous resistance parameters $\{R_{\mathrm{a}}, R_{\mathrm{s}}, R_{\mathrm{v}}\}$ are calculated from average values of flow (CO) and pressure using Eq. (2). The aortic valve resistance R_{av} is calculated from approximations of maximal left ventricular volume and pressure, while the minimum valve resistance R_{mv} is calculated from the minimum left ventricular pressure.

The arterial and venous elastances $\{E_{\mathrm{ao}}, E_{\mathrm{a}}, E_{\mathrm{vc}}, E_{\mathrm{sv}}\}$ are calculated from Eq. (3), while nominal minimum E_{m} and maximum E_{M} elastance of the left ventricle in Eq. (4) are computed as

$$E_{\mathrm{m}} = \frac{\mathrm{avg}(p_{\mathrm{lv,dia}})}{\mathrm{avg}(V_{\mathrm{lv,dia}}) - V_{\mathrm{lv,0}}} \tag{6}$$

$$E_{\mathrm{M}} = \frac{\mathrm{avg}(p_{\mathrm{lv,sys}})}{\mathrm{avg}(V_{\mathrm{lv,sys}}) - V_{\mathrm{lv,0}}}. \tag{7}$$

Here the minimum and maximum are taken over all cycles during baseline (before each blood withdrawal).

Similar to previous studies [21,34], we assume that the timing parameters $\alpha_{\mathrm{s}} = T_{\mathrm{s}}/T$ and $\alpha_r = T_r/T$ used to compute the time-varying elastance $E_{\mathrm{lv}}(t)$ are constant.

2.3.5 Initial conditions

Assuming that model simulation begins at the end of systolic contraction (at the beginning of diastolic filling), we set the initial value of the left ventricular volume to its maximum value. Initial conditions for the arterial and venous volume are set to their stressed volume (V_i) given in Table 3.

2.4 Model analysis

The objective of this study is to estimate model parameters to fit the model output (left ventricular volume and pressure) to data. The most important components of the experimental data for the model to replicate are the maximum and minimum V_{lv} and p_{lv} of each cardiac cycle. Therefore, the error in the maximum and minimum V_{lv} and p_{lv} of each cardiac cycle are explicitly included in the cost function along with the overall error in the model fit to the data. Specifically, we minimize the least squares error $J = r^T r$,

$$r = \left[\xi \Delta p_{\mathrm{lv}}, \xi \Delta p_{\mathrm{lv,max}}, \xi \Delta p_{\mathrm{lv,min}}, \Delta V_{\mathrm{lv}}, \Delta V_{\mathrm{lv,max}}, \Delta V_{\mathrm{lv,min}}\right] \tag{8}$$

where $\Delta X = \{(X_{i,\mathrm{Data}} - X_{i,\mathrm{Model}})/\sqrt{N}\}$, $i = 1 \ldots N$ with N the number of measurement points in the signal, and ξ is a weight factor introduced to scale the magnitude of the pressure compared to that of the volume (e.g., for blood withdrawal 2, $\xi = 2$).

Optimization is done using the nonlinear programming solver `fmincon` in MATLAB with the interior point algorithm. Whenever possible, we make use of the parallel capability of `fmincon` optimization and use MATLAB's Parallel Computing Toolbox to improve computational efficiency.

Given that data are only available from one compartment, similar to previous studies [21,25,34] we use sensitivity analysis and covariance-based subset selection methodology to determine a set of identifiable parameters that can inform the model.

2.4.1 Sensitivity analysis and covariance-based subset selection

To study the changes in the model output with respect to the parameters, similar to previous studies [21,34], we use local sensitivity analysis at baseline before BW1. The sensitivity matrix is defined as

$$S_{i,j} = \frac{\partial r_i(\theta)}{\partial \theta_j},$$

where r is the model residual as in Eq. (8), and θ_j is the jth parameter.

The entries in the sensitivity matrix are calculated numerically using a forward difference approximation and are evaluated locally at the nominal parameter values [27].

Ranked sensitivities for each parameter j

$$\tilde{S}_j = \left| \frac{\partial r_i(\theta)}{\partial \theta_j} \right|_{L^2}$$

are computed by averaging the time-varying sensitivities over time using the L^2-norm allowing us to separate sensitivities into two groups: sensitive and insensitive.

From the sensitive parameter set, we determine a subset of identifiable parameters using the structured correlation method [21,23,25]. This method systematically removes the least sensitive correlated parameter from the correlation matrix. The first step is using the sensitivity matrix to calculate the Fisher Information Matrix ($F = S^T S$). The inverse to the Fisher Information Matrix is the covariance matrix ($C = F^{-1}$), and finally the correlation matrix is given as

$$c_{i,j} = \frac{C_{i,j}}{\sqrt{C_{i,i} C_{j,j}}}.$$

Correlated parameters are removed until $c_{i,j} < \epsilon$ for all i, j; we set a threshold at $\epsilon = 0.8$.

2.4.2 Parameter confidence intervals

To assess the robustness of the estimated identifiable parameter values, we calculate confidence intervals using the Fisher information matrix, assuming that variance is i.i.d. as $\mathcal{N}(0, \sigma^2)$ [7]. Then $\hat{\theta} \sim \mathcal{N}(\theta, \sigma^2)$, where θ is the unknown true parameter set and $\hat{\theta}$ is an estimator of θ. The confidence interval for the j^{th} element of $\hat{\theta}$ is given by

$$CI_j = \hat{\theta}_j \pm t_{N-q}^{\alpha/2} \, s \, \sqrt{C_{jj}} = \hat{\theta}_j \pm \Delta\theta_j,$$

where N is the total number of data points, q is the number of estimated parameters, $t_{N-q}^{\alpha/2}$ is the t-value for the $1 - \alpha/2$ quartile with $N - q$ degrees of freedom, and $s^2 = J(\hat{\theta})$ is an estimator of the variance σ^2.

3 Simulations

The model described above was first solved at baseline estimating the subset of identifiable parameters (assumed constant) and then run during blood withdrawal estimating time-varying parameters regulated by the cardiovascular control system. This was repeated for each blood withdrawal adjusting the calculation of nominal parameter values, accounting for the blood withdrawn in the previous cycle.

3.1 Baseline

To ensure that the model behaves appropriately, we first estimate constant baseline parameters minimizing the mean squared error between the model predictions and data. We first use sensitivity analysis and covariance-based subset selection methodology based on nominal parameters to determine a set of identifiable parameters that are subsequently estimated. Then, to ensure the oscillations of the model output are in phase with the data, we shift data in time and estimate the identifiable parameters at each time shift. From these we choose the shift associated with the smallest mean squared error and apply this shift to the entire data segment including both baseline and blood withdrawal. This process is repeated for each blood withdrawal adjusting calculation of nominal parameter values to account for the blood withdrawn in the previous cycle.

3.2 Blood withdrawal

Each blood withdrawal simulation is initiated using the estimated baseline parameters. A description follows of how to model blood withdrawal and introduce parameter estimation procedures for determining time-varying parameters.

3.2.1 Modeling blood withdrawal

To simulate hemorrhagic trauma, similar to the experimental setting, we withdraw blood from the systemic arteries at a constant rate,

$$\frac{\mathrm{d}V_{\mathrm{sa}}}{\mathrm{d}t} = q_{\mathrm{a}} - q_{\mathrm{s}} - q_{\mathrm{out}}, \tag{9}$$

where

$$q_{\mathrm{out}} = \begin{cases} \frac{\mathrm{Vol}}{t_E - t_S}, & t_S \le t \le t_E \\ 0, & \text{otherwise.} \end{cases}$$

Here Vol corresponds to the blood volume withdrawn in the experiment, t_S and t_E denote the start and end times of the blood withdrawal, and q_{out} denotes the blood withdrawal rate. For the data used here, the volumes of blood withdrawn vary from the 1–2 ml (see Table 1), with 30% withdrawn from the stressed volume and 70% from the unstressed volume. For the first and fourth blood withdrawal, the blood is withdrawn at a constant rate, while the second and third blood withdrawals consist of two consecutive constant-rate withdrawals (see Table 1).

3.2.2 Time-varying response: splines

The cardiovascular control system regulates vascular resistance, cardiac contractility, and heart rate [3]. Heart rate is an input for the model; to account for variations in the other quantities regulated by the cardiovascular control system, we represent them as time-varying parameters using piecewise linear functions that depend on time as in [22,34], where

$$X(t) = \sum_{i=1}^{N} \gamma_i K_i(t),$$
$$K_i(t) = \begin{cases} \dfrac{t - t_{i-1}}{t_i - t_{i-1}}, & t_{i-1} \le t \le t_i \\ \dfrac{t_{i+1} - t}{t_{i+1} - t_i}, & t_i \le t \le t_{i+1} \\ 0, & \text{otherwise} \end{cases} \tag{10}$$

Here N denotes the number of time nodes along the piecewise linear spline. The coefficients γ_i for $i = 1 \ldots N$ are estimated using nonlinear optimization. $X(t)$ denotes the time evolution of time-varying parameter X. As noted in [22,34], this method requires that the number of nodes N and their spread along the time span are specified a priori.

In this study, for the first and last 20 s of data we placed a node every 5 cardiac cycles, while for the remaining data we placed one node every 15 cycles. Placing nodes relative to the length of the cardiac cycle ensures that the number of nodes are higher during elevated heart rate, allowing us to better capture time-varying responses. Moreover, including more nodes at the beginning and end of the time interval minimizes the effect of oscillations at the boundary.

3.2.3 Time-varying response: functional forms

Given the optimal piecewise linear splines described above, we seek to express the time-varying dynamics as functions of aortic pressure and left ventricular volume. Connecting the dynamics of the time-varying parameters back to the controller input can provide insight into the mechanisms at work in cardiovascular regulation.

Cardiovascular regulation occurs on a timescale that corresponds to 5 to 10 heartbeats [24], which here is on the order of 1.5–3 s and is much shorter than the timescale considered in this experiment (the blood withdrawals last 20–45 s). Therefore, we simplify the system by assuming the parameters modified by cardiovascular regulation are in quasi-steady state.

As a first approach, we assume that the controlled parameters can be represented by a sigmoid function of the form

$$X(t) = \frac{X_2 - X_1}{1 + \exp\left(-\dfrac{\bar{p}_{\text{ao}}(t) - p}{z}\right)} + X_1, \tag{11}$$

where the moving average of aortic pressure is calculated as a numerical solution equal to

$$\frac{\mathrm{d}\bar{p}_{\text{ao}}}{\mathrm{d}t} = \alpha(p_{\text{ao}} - \bar{p}_{\text{ao}}), \tag{12}$$

with $\alpha = 0.5$. The parameters in Eq. (11) correspond to:

- X_1 and X_2, the asymptotes of the sigmoid, either the minimum and maximum values for an *increasing* function of $\bar{p}_{\text{ao}}$, or the maximum and minimum values for a *decreasing* function of $\bar{p}_{\text{ao}}$;
- p, the half-saturation aortic pressure value; and
- z, the sensitivity of X to $\bar{p}_{\text{ao}}$.

We use the value of X estimated from baseline optimizations (X_B) to eliminate one free parameter by setting $X(t_0) \equiv X_B$, where t_0 is the initial time of the baseline data, which is assumed to be at steady state. This implies that

$$X_2 = (X_B - X_1)\left(1 + \exp\left(-\frac{\bar{p}_{\text{ao}}(t_0) - p}{z}\right)\right) + X_1.$$

For parameters that cannot be represented as a function of pressure only, we propose to let

$$X(t) = a\bar{p}_{\text{ao}}(t) + b\bar{V}_{\text{lv}}(t) + c, \tag{13}$$

where similar to pressure, the moving average of left ventricular volume is the solution to

$$\frac{\mathrm{d}\bar{V}_{\text{lv}}}{\mathrm{d}t} = \alpha(V_{\text{lv}} - \bar{V}_{\text{lv}}), \tag{14}$$

with $\alpha = 0.5$. The constraint $X(t_0) \equiv X_B$ at the initial time of the baseline data gives

$$c = X_B - a\bar{p}_{\text{ao}}(t_0) - b\bar{V}_{\text{lv}}(t_0).$$

These functional forms were fit to the optimized linear splines for each time-varying parameter. The rationale in assigning different functional forms to the various time-varying parameters is addressed in Sect. 5.

3.2.4 Simulation procedure: overview

In summary, our approach to understanding the cardiovascular response to multiple hemorrhages illustrated in Fig. 3 requires

- calculation of nominal parameter values and initial conditions, accounting for the amount of blood withdrawn in the previous cycle;

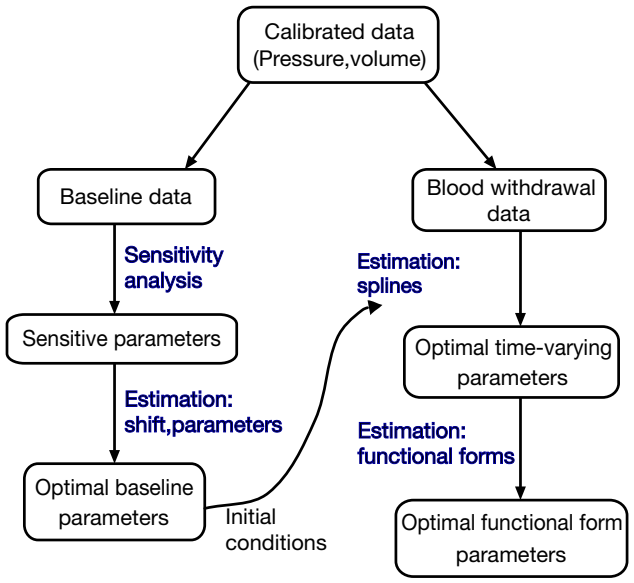

Fig. 3 Cardiovascular regulation in response to multiple hemorrhages. The calibrated data (left ventricular pressure and volume) consist of a baseline phase (preceding hemorrhage) and a blood withdrawal phase. The baseline phase is used for sensitivity analysis, to determine a set of identifiable parameters, and for optimization estimating constant values for the identifiable parameters R_s, E_m, E_M, α_s, α_r. These parameters are used as initial conditions for optimization of time-varying parameters E_m, E_M, R_s regulated by the cardiovascular control system. The time-varying parameters are subsequently analyzed using mechanistic functional forms to assess how the cardiovascular control system adapts to hemorrhage

- determination of a subset of identifiable parameters (sensitivity analysis and covariance-based subset selection for the baseline data with nominal parameters);
- hand-fitting to align data to the model predictions for each blood withdrawal;
- optimization to estimate an optimal time shift along with constant baseline parameters and their confidence intervals for each blood withdrawal;
- estimation of the spline nodes (used to compute piecewise linear function) for parameters regulated by the cardiovascular control system for each blood withdrawal;
- estimation of functional models, providing mechanistic insight into the changes in parameters with successive withdrawals.

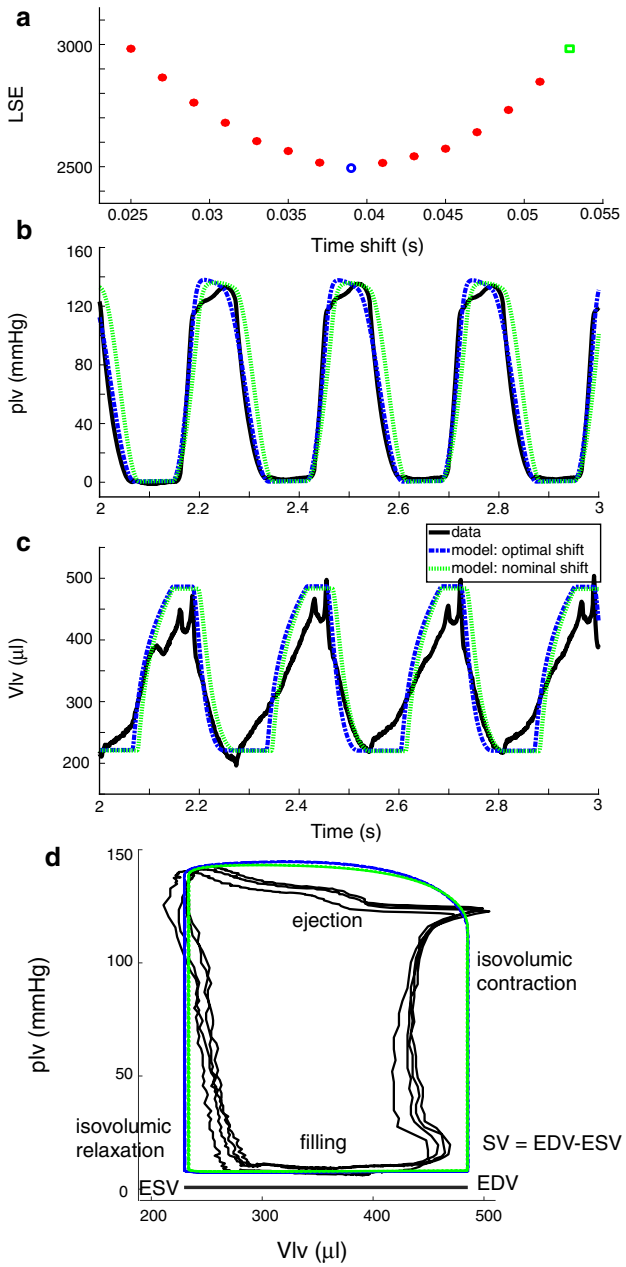

Fig. 4 Data (black) and baseline model predictions of left ventricular pressure (**b**), volume (**c**), and pressure-volume loop (**d**). Green dashed line shows results with nominal shift and blue with optimal shift. **a** Least squares error over a range of time shifts (green square: nominal shift; blue circle: optimal shift) (colour figure online)

4 Results

4.1 Baseline

Sensitivity analysis and covariance-based subset selection revealed that we can estimate five parameters (R_s, E_m, E_M, α_s and α_r) minimizing the mean squared error between model predictions and data. Results further showed that it is possible to identify an optimal time shift. As in [21], we manually choose an initial guess for this shift and then repeat the optimizations in parallel for a large range of nearby shift values. Figure 4a shows that for blood withdrawal 2, the mean squared error is minimized by a time shift $\delta t = 0.039$ s. Figure 4b–d shows the improved fit to the data predicted with this optimum time shift, compared to our nominal shift value $\delta t = 0.019$ s. We achieved similar results for the other three

Table 4 Optimized identifiable baseline parameter values, confidence intervals, and mean square error associated with the baseline preceding blood withdrawal BWi, $i = 1 \ldots 4$

Parameter	BW1	BW2	BW3	BW4
α_s	$0.401 \pm 8.32\text{E}{-4}$	$0.426 \pm 6.55\text{E}{-4}$	$0.292 \pm 8.93\text{E}{-4}$	$0.112 \pm 1.7\text{E}{-3}$
α_r	$0.710 \pm 1.35\text{E}{-5}$	$0.722 \pm 1.13\text{E}{-5}$	$0.747 \pm 1.41\text{E}{-5}$	$0.953 \pm 6.0\text{E}{-5}$
E_m (E−3)	4.35 ± 1.1	4.29 ± 0.99	4.39 ± 0.87	1.24 ± 0.83
E_M	$0.788 \pm 2.5\text{E}{-3}$	$0.785 \pm 2.1\text{E}{-3}$	$0.542 \pm 1.7\text{E}{-3}$	$0.208 \pm 1.2\text{E}{-3}$
R_s	$0.114 \pm 8.56\text{E}{-4}$	$0.115 \pm 9.66\text{E}{-4}$	$0.105 \pm 9.31\text{E}{-4}$	$0.059 \pm 1.2\text{E}{-3}$
J (E+3)	2.92	2.58	2.71	2.55

blood withdrawals, and the mean squared cost for these is included in Table 4.

The optimized values for the five identifiable parameters, the corresponding confidence intervals, and the mean square error J are given in Table 4 for all four baseline segments. Except for E_m, all confidence intervals are at least an order of magnitude smaller than the parameters. The confidence interval for E_m may be relatively large because E_m is small in magnitude.

4.2 Blood withdrawal

4.2.1 Time-varying response: splines

As noted earlier, the cardiovascular control system regulates heart rate (model input), systemic vascular resistance, and cardiac contractility. During baseline, we found five identifiable parameters, and of these three correspond to quantities regulated by the cardiovascular control system: systemic vascular resistance, represented by R_s, and maximum and minimum cardiac contractility, denoted E_M and E_m. Therefore, these three parameters are allowed to vary to best examine the response to blood withdrawal.

The constant parameters optimized in the baseline simulations preceding each blood withdrawal provide initial guesses for the spline optimization. A sample fit of the left ventricular pressure and volume for the second blood withdrawal is shown in Fig. 5. The model predictions show good agreement with the data both during the withdrawal and during the recovery time, a portion of which is magnified in the insert. The fits to data for blood withdrawals 1, 3 and 4 also show good agreement and are provided in the Electronic Supplementary Material. The mean squared error J for all blood withdrawals is listed in Table 5.

The time-varying parameters estimated for each blood withdrawal are plotted in Fig. 6. Figure 6a depicts the time evolution of the systemic vascular resistance R_s, and Fig. 6b depicts cardiac contractility ($E_M - E_m$) over all four blood withdrawals. For each blood withdrawal, our results predict consistent behavior. Both quantities first decrease and then increase. In addition, both quantities decrease with successive blood withdrawals. The only exception is the prediction of contractility in blood withdrawal 4, which rapidly increases at the end of the experiment. This could be a result of the fact that the left ventricular volume initially recovers to a steady-state value but then plummets at the end of the experiment (see Fig. 1).

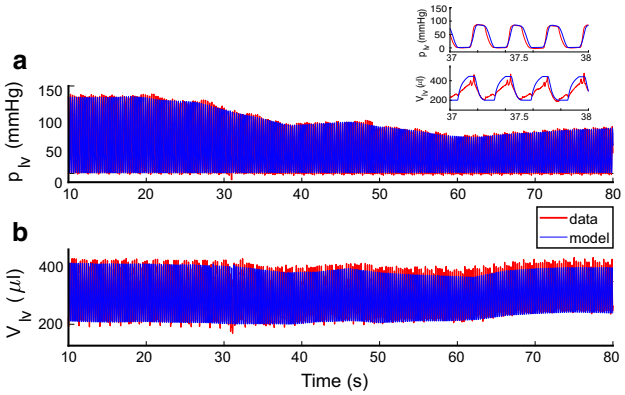

Fig. 5 Fit of left ventricular pressure p_{lv} (**a**) and left ventricular volume V_{lv} (**b**) for the second blood withdrawal. Data are marked with red lines and model predictions with blue lines. Inset: zoom of the fit over a short time interval during the blood withdrawal. For this fit, $J = 5.02\text{E}{+3}$. Optimization results for the remaining blood withdrawals are included in the Electronic Supplementary Material (colour figure online)

4.2.2 Time-varying response: functional forms

As stated earlier, we use mechanistic functional forms to capture the dynamics of the splines for R_s, E_m, and E_M. Figure 7 illustrates the good agreement between the functional forms and the splines, for the second blood withdrawal. The expressions for the functional forms are given in Eqs. 11 and 13. As described earlier, the controlled parameters are predicted as functions of mean aortic pressure $\overline{p}_{ao}$ and mean ventricular volume $\bar{V}_{lv}$ (Fig. 7d, e). The full set of estimated parameters for functional forms is given in Table 5.

Results show that aortic pressure alone is enough to replicate the splines for R_s and E_m, but another input $\bar{V}_{lv}$ is needed to replicate E_M. Additionally, it is interesting to note that the aortic pressure and left ventricular volume act independently and additively. More discussion is given in Section 5.

Table 5 Functional form parameters for variables R_s, E_m, E_M and the minimum cost $J = r^T r$ for fit to respective spline

Param				R_s BWs 1–4
X_1 (E−3)				1.08
X_2				0.130
p				48.6
z				37.4
J (E−3)				5.45
	E_m			
	BW1	BW2	BW3	BW4
X_1 (E−3)	5.1	5.9	10.9	4.5
X_2	0.0042	0.0043	0.0040	−16.22
p	108.3	65.9	20.0	170.0
z	9.49	10.0	28.7	15.1
J (E−2)	0.69	2.09	1.64	3.30
	E_M			
	BW1	BW2	BW3	BW4
a (E−3)	7.29	9.44	6.04	8.92
b (E−3)	−3.21	−3.73	−1.11	−2.64
c	0.950	0.879	0.310	0.666
J (E−3)	4.71	5.94	1.20	3.46

For the functional forms, $r = \{(F_i - S_i)/(\max(S) - \min(S))/\sqrt{N}\}$, $i = 1 \ldots N$ where F is the functional form, S is the spline, and N the number of time points

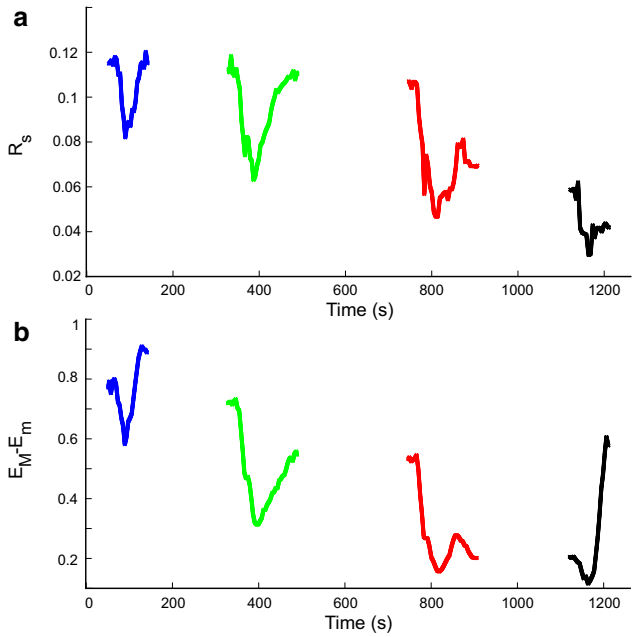

Fig. 6 Predicted time evolution of systemic vascular resistance R_s (**a**) and cardiac contractility $E_M - E_m$ (**b**) over the four blood withdrawals. Breaks in the graphs correspond to steady-state times when no blood is withdrawn

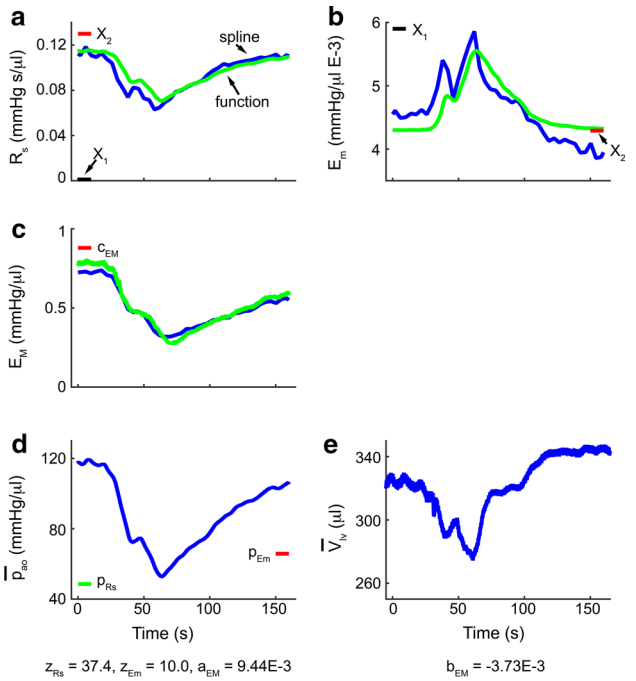

Fig. 7 Computed experimental splines and functional predictions for blood withdrawal two. The systemic vascular resistance R_s (**a**) and minimum elastance E_m (**b**) are modeled as functions of mean aortic pressure $\bar{p}_{ao}$ (**d**) using (11), with the half-saturation value p_2 and sensitivity z indicated. The maximum elastance E_M (**c**) is modeled as a linear function of the mean aortic pressure $\bar{p}_{ao}$ (**d**) and the mean left ventricular volume $\bar{V}_{ao}$ (**e**) using (13). Blue lines denote results from spline predictions of the time-varying parameters and the green lines denote model-based predictions (colour figure online)

Finally, we note that coupling the five-compartment cardiovascular model with the optimized functional forms for the time-varying parameters give good agreement with data. Results of this simulation are both visually similar and have a similar mean squared error, J, to Fig. 5, and a sample is included in the Electronic Supplementary Material.

5 Discussion

The analysis methodology presented here provides a general approach that can be used when a mechanistic time evolution model is used to describe the response of a biological system to a perturbation from steady state. First, the mathematical model is developed to represent the dynamics based on a mechanistic understanding of the biological system. Then the nominal parameters in the model are computed from a combination of our knowledge of the system and directly from the data at baseline. In the neighborhood of the nominal parameter values, sensitivity analysis and covariance-based subset selection methodology were used to identify the most sensitive parameters. In the system presented here, we find that during the perturbation and response some of the system

dynamics are embedded in certain parameters in this subset. Allowing these parameters to vary in time can give insight into the response when prior knowledge about their evolution is not available.

To illustrate this analysis methodology, we apply this approach to describe the response of the cardiovascular system to a series of hemorrhage events, represented by a lumped parameter model of cardiovascular dynamics. Using heart rate as an input, this model is fitted to measurements of left ventricular volume and pressure. We identify five model parameters estimated at steady state of which three are allowed to vary to predict the response to blood withdrawal: systemic vascular resistance (R_s) and cardiac contractility (E_M, E_m). Finally, we develop functional forms estimating dynamics of controlled variables as functions of aortic blood pressure and left ventricular volume. Despite the fact that we use one dataset in this study, our analysis illustrates how the cardiovascular control system may respond to multiple blood withdrawals. More studies are needed, analyzing more datasets, to confirm if the observed dynamics are replicated across individuals.

5.1 Baseline simulations

Our simulations of the baseline data prior to each of the four blood withdrawals (Fig. 4 illustrating baseline prior to blood withdrawal 2) reproduce the pulsatile behavior of the left ventricular pressure and volume. These results were obtained estimating five parameters ($\alpha_s, \alpha_r, E_m, E_M$ and R_s) that were found (using sensitivity analysis and covariance-based subset selection methodology) to inform the data. To obtain an optimal fit, in addition to estimation of model parameters, we estimated an optimal time shift allowing us to accurately align the model to data (as illustrated in Fig. 4a). The latter was done by estimating the least squares error over a large number of time shifts. While this is more time-consuming than estimating initial conditions along with identifiable parameters, it prevented addition of non-identifiable parameters that could not be informed by the data. An alternative approach would have been to include this time shift as another parameter to be estimated in the baseline optimization; in our experience, this is generally more time-consuming than the approach utilized here.

The proposed model is able to capture the general form of the experimental measures of the left ventricular pressure and volume; however, small features present in the data are not reproduced. The artifacts in the volume measurement occur during the isovolumetric contraction just after the closing of the mitral valve (shown in Fig. 4d). These artifacts can be explained by movement of the pressure-volume catheter within the chamber during this portion of the cardiac cycle, causing variation in the fraction of the conductance transmitted through the myocardial tissue. The small features in maximal pressure not captured by the model may be a result of our simple model formulation not including the pulmonary circuit and the left atrium, the interaction between chambers of the heart, or the complex dynamics of the aortic and mitral valves. Given our objective, to study how the control system reacts to blood withdrawal on a time scale much longer than a cardiac cycle, we believe that these discrepancies are not significant for this study.

It is worth noting that the optimization for the baseline parameters is robust to initial guesses varying within 20% of the nominal parameter values (results not shown). The values of α_s and α_r do not vary appreciably across the baselines, prior to each of the four blood withdrawals (except for blood withdrawal 4, see Table 4) indicating long-term accommodation does not shift the left ventricular time spent in the contractile and relaxed stages, as a fraction of each beat.

This baseline analysis is used to set the initial values for the time-varying parameters (E_m, E_M and R_s) which decrease with each successive blood withdrawal as shown in Fig. 6.

5.2 Blood withdrawal

In the present study, we assume that 30% of the blood is withdrawn from the stressed blood volume while the remainder comes from the unstressed volume; in q_{out} (defined in (9)) V_{tot} reflects 30% of each 1 ml withdrawal. This agrees with results in previous studies, which suggest similar divisions estimating that 25–40% is withdrawn from the stressed volume [12,13,20]. In this computational model, only the stressed volume is circulated; therefore, we directly withdraw the 30% of the volume from the systemic arteries. In this study, we assumed that blood was withdrawn at a constant rate. To test this, we compared results to models withdrawing blood at different rates (including linearly and exponentially decreasing rates). As these more involved models with additional parameters did not significantly improve predictions, we reverted to the simplified assumption of constant withdrawal rate over each period.

It is well-documented that autonomic regulation is driven by baroreceptor signals originating in the aortic arch and carotid arteries which respond to changes in blood pressure within each of these vessels [8]. Afferent signals are integrated in the nucleus solitary tract. From there activity in parasympathetic and sympathetic efferent fibers influence heart rate, cardiac contractility, and peripheral vascular resistance [9]. At baseline, we identified five parameters; of these, three are modulated by the autonomic control system: R_s representing systemic vascular resistance and E_M and E_m associated with cardiac contractility ($c = E_M - E_m$). The last parameter controlled is heart rate, which is implicitly accounted for as it is an input to the cardiovascular model. Given that blood withdrawal experiments are done over longer time intervals (90–180 s) the cardiovascular

system control includes both fast autonomic response and a slower passive response. Several studies have developed functional models for the former, while the latter is more difficult to characterize. As a result, we used piecewise linear splines to study how systemic vascular resistance and cardiac contractility vary within and across blood withdrawals. The variations captured by these splines were subsequently modeled using functional expressions derived to study how systemic vascular resistance and cardiac contractility are controlled through feedback mechanisms.

Predicting the time evolution of these parameters using the spline method is computationally expensive. However, utilizing parallel computing and starting with initial conditions informed by the baseline helps speed up computations. An alternative approach is to use nonlinear Kalman filtering [22] to estimate the time-varying parameters, which has the advantage that it also provides information on the model variance. Yet Kalman filtering can be difficult to use in this type of problem, as the filter easily can get stuck tracking dynamics within a pulse rather than tracking the long-time scale dynamics. In future studies, we plan to put more effort into developing a filter (expanding the method in [22]) for the problem studied here.

Despite only being identified for one dataset, the time-varying predictions of the controlled parameters (R_s, E_M, and E_m) give insight into cardiovascular system function, which cannot be measured experimentally. In Fig. 6, the systemic resistance R_s and E_M decrease acutely during each blood withdrawal followed by an increase mediated by the autonomic control system, while E_m displays the opposite behavior. In addition, R_s and E_M decrease chronically over the four blood withdrawals, while E_m increases (not shown).

Acutely within each blood withdrawal, the response of the systemic resistance, R_s, can be explained from the perspective of perfusion. As pressure drops initially, the only way to maintain cardiac output and perfusion in the tissues is for systemic resistance to drop along with pressure. This is observed here and in previous studies [34]. The mechanism for this drop in R_s is not clear; however, the myogenic response in the systemic vasculature could drive a drop in R_s with a drop in pressure and would respond fairly rapidly to the intraluminal pressure [15]. After this initial drop in R_s, our simulations indicate that the autonomic system tries to bring the pressure back to baseline by increasing R_s. As a result, pressure increases and perfusion is maintained. On the longer time scale from blood withdrawal to blood withdrawal, the systemic resistance is seen to chronically drop. This can also partially be explained by the myogenic response of the vasculature to pressure. In addition, some tissues take a larger portion of the cardiac output to maintain perfusion (e.g., cardiac tissue) [11]. Vasculature in these tissues must dilate, reducing their tissue vascular resistance, to increase their share of the cardiac output. Since each tissue bed is in parallel with all others, the resistance in these vasculatures dominates the lumped value of overall systemic resistance, represented by R_s. This same phenomenon has also been observed in a previous experimental study [14].

The contractility of the left ventricle is the difference $c = E_M - E_m$, proportional to the maximum elastance E_M. An increase in E_M corresponds to an increased contractility, and this is thought to occur through autonomic regulation as the blood pressure decreases. Our results show that E_M first drops and then increases. Again, this parameter is controlled by the sympathetic response and will reflect the same delay observed in R_s. The minimum elastance of the left ventricle E_m shows an increase during the blood withdrawals followed by return to baseline. Yet, since $E_M \gg E_m$, E_m does not contribute considerably to the cardiac contractility range $E_M - E_m$ in Fig. 6. On the other hand, E_m plays an essential role during filling; a decrease in E_m increases left ventricular filling. This is counter to our observations here; however, the value of E_m is quite small and the changes observed may not be determined accurately with the given dataset.

On the longer time scale, cardiac contractility ($c = E_M - E_m$) decreases chronically over the four blood withdrawals. The contractility does not return to the baseline value in withdrawals 2 and 3 (see Fig. 6). The reduction in contractility may be explained by a reduced left ventricular filling causing a change, passive and active properties regulating the maximal elastance of the ventricle. The results shown in Fig. 6 reflect that the changes in active and passive properties from the loss of blood counteract the autonomic increase in heart contractility and result in an overall reduction in contractility both acutely and chronically as more blood is withdrawn. In the fourth withdrawal, the contractility increases dramatically, but it is not clear whether this increase is an overshoot or reflects a large change in the autonomic response. At this stage, the rat was not able to tolerate additional blood withdrawals.

5.3 Functional forms and autonomic regulation

The time-varying responses of E_M, E_m and R_s that produce a good characterization of the experimental data have been cast in a functional form to understand how the time-varying response depends on the input to the cardiovascular system. As mentioned previously, autonomic regulation is driven by pressure sensors located in the aortic arch and carotid artery [5,9]. Therefore, we developed a sigmoid functional form for the dynamics of the time-varying parameters, E_M, E_m and R_s, in terms of the mean aortic pressure $\bar{p}_{ao}$ and mean left ventricular volume $\bar{V}_{lv}$. Note that in our cardiovascular model, the pressure at the carotid artery is assumed to be identical to that at the aortic arch since these vessels are in close proximity in supine position. We find that R_s and

E_M decrease following the dynamics of $\bar{p}_{ao}$ at the beginning of a blood withdrawal and then recover at the end of the withdrawal, while E_m increases then decreases. Except for E_M, parameter dynamics could be predicted as a function of only $\bar{p}_{ao}$, indicating that autonomic system alone controls the response. For E_M we found that it was necessary to include a dependence on $\bar{V}_{lv}$. We hypothesize that the dependence on $\bar{V}_{lv}$ is caused by reduced filling of the ventricles leading to a weaker contraction (as predicted by the Frank–Starling effect [26]). This observation suggests that a change in the passive and active properties must occur to predict the acute and steady-state reduction in contractility.

The functional forms corresponding to individual blood withdrawals can be used to represent autonomic regulation during that specific blood withdrawal. However, if the parameters of the functional forms remain constant across multiple blood withdrawals, this indicates that the systemic relationship is invariant in autonomic regulation. Thus, our ability to fit R_s across all four blood withdrawals using a single set of parameters (see Table 5) suggests that autonomic regulation of systemic resistance is not altered during severe hemorrhaging and is solely a function of autonomic regulation responding to $\bar{p}_{ao}$, or at least on the timescale considered here.

Unlike R_s, the minimum elastance E_m does not follow a consistent trend across all blood withdrawals. The numerical values of the splines for E_m increase across successive blood withdrawals until the fourth, where the dramatic drop in the splines for E_m does not correspond to the trend in aortic pressure. As a result, we were unable to find a unique set of parameters to fit E_m across all four blood withdrawals. Two possible explanations for the interesting behavior of E_m throughout multiple hemorrhages are that autonomic regulation of E_m is biphasic in terms of $\bar{p}_{ao}$ (which we do not account for in our functional forms), or that E_m may be correlated with other time-varying parameters, such as E_M or R_s. If E_m is correlated with other time-varying parameters, the splines we calculated for its evolution would not be unique and may not completely characterize autonomic regulation of this parameter across multiple hemorrhages. We plan to further investigate the cause of the complicated behavior seen in the minimum heart elastance E_m.

In modeling the dynamics of E_M, we initially used sigmoidal functions similar to those used for R_s. However, when fitting sigmoids to splines for E_M, we found the parameters of the sigmoid functions to be highly correlated. As a result, we were unable to identify unique parameters for the functional forms. Therefore, we use the linear functions in Eq. (13). We suspect autonomic regulation of E_M is truly nonlinear, but a linear approximation is valid because the dynamics seen in the experiments span only a small range of the autonomic response of E_M.

5.4 Limitations and future studies

This study was performed based on experimental data obtained prior to performing the analysis presented here. Several changes should be made if this experiment is repeated. First of all, saline calibrations for the conduction catheter should be performed both prior to and after the series of blood withdrawals to track how the blood conductivity changes over the course of the experiment. This could possibly eliminate the use of literature values for the determination of the volume calibration. In addition, a pressure catheter in the right heart measuring pulmonary pressures, and measurements of aortic pressures could provide additional data to inform the model allowing more robust identification of model parameters.

Finally, the parameters within the functional forms for systemic resistance and cardiac elastance were estimated against the spline output. In future studies, we plan to estimate identifiable parameters defining the functional forms, to confirm that the time-varying quantities can predict observed output. We also plan to repeat the simulations for multiple mice, increasing the sample size.

6 Conclusion

In the present work, we propose methods for studying the change in autonomic regulation in the cardiovascular system upon examination of data across multiple blood withdrawals in a model organism. Specifically, we use a five-compartment differential equations model to predict left ventricular pressure and volume during baseline and during hemorrhage and the return to steady state. Our sensitivity analysis of the model parameters indicates that characteristics of cardiac contractility and vasoconstriction may be controlled during the stress of blood loss. In our model, aortic pressure and left ventricular volume are inputs to the autonomic response to the hemorrhage stress.

Funding This material is based upon work supported by the Mathematics Research Communities of the American Mathematical Society, under National Science Foundation Grant Number DMS 1321794. The project was initiated during the Mathematics Research Community on Mathematics in Physiology and Medicine workshop (2016). Follow-up visits and workshops were supported by the John N. Mordeson Endowed Chair in Mathematics at Creighton University and by the Mathematical Biosciences Institute. In addition, MVC was supported in part by the Mathematical Biosciences Institute and the National Science Foundation under Grant Number DMS 1440386, and by NSF Grant Number DMS 1408742. SSD was supported by a Joint University of California Davis and Lawrence Livermore National Laboratory Graduate Mentorship Award. CD, BEC and MSO were been supported in part by NIH NIGMS Grant Number P50-GM094503-02, and CD was supported by was supported by the U.S. Department of Veterans Affairs BLR&D program by a Merit Review Award # BX001863. CD and BEC were also supported by NIH NHLBI Grant Number U01 HL109505-01.

Compliance with ethical standards

Conflict of interest The authors declare that they have no conflicts of interest.

Ethical approval All applicable international, national, and/or institutional guidelines for the care and use of animals were followed. All procedures performed in studies involving animals were in accordance with the ethical standards of the institution at which the studies were conducted.

Data The datasets generated during and/or analyzed during the current study are available on request from the corresponding author.

Appendix: Cardiovascular model equations

We provide here the complete set of equations for the five-compartment cardiovascular model proposed above and summarized in Fig. 2. The evolution of each compartment's volume is given by:

$$\begin{aligned}
\frac{\mathrm{d}V_{\mathrm{ao}}}{\mathrm{d}t} &= q_{\mathrm{av}} - q_{\mathrm{a}} \\
\frac{\mathrm{d}V_{\mathrm{sa}}}{\mathrm{d}t} &= q_{\mathrm{a}} - q_{\mathrm{s}} - q_{\mathrm{out}} \\
\frac{\mathrm{d}V_{\mathrm{sv}}}{\mathrm{d}t} &= q_{\mathrm{s}} - q_{\mathrm{v}} \\
\frac{\mathrm{d}V_{\mathrm{vc}}}{\mathrm{d}t} &= q_{\mathrm{v}} - q_{\mathrm{mv}} \\
\frac{\mathrm{d}V_{\mathrm{lv}}}{\mathrm{d}t} &= q_{\mathrm{mv}} - q_{\mathrm{av}}
\end{aligned}$$

Note that this corresponds to the blood withdrawal simulations where the withdrawal rate is q_{out}. The flow between compartments is given by:

$$\begin{aligned}
q_{\mathrm{av}} &= \begin{cases} \dfrac{p_{\mathrm{lv}} - p_{\mathrm{ao}}}{R_{\mathrm{av}}}, & p_{\mathrm{lv}} > p_{\mathrm{ao}} \ \text{(open valve)} \\ 0, & \text{otherwise} \end{cases} \\
q_{\mathrm{s}} &= \frac{p_{\mathrm{sa}} - p_{\mathrm{sv}}}{R_{\mathrm{s}}} \\
q_{\mathrm{v}} &= \frac{p_{\mathrm{sv}} - p_{\mathrm{vc}}}{R_{\mathrm{v}}} \\
q_{\mathrm{a}} &= \frac{p_{\mathrm{ao}} - p_{\mathrm{sa}}}{R_{\mathrm{a}}} \\
q_{\mathrm{mv}} &= \begin{cases} \dfrac{p_{\mathrm{vc}} - p_{\mathrm{lv}}}{R_{\mathrm{mv}}}, & p_{\mathrm{vc}} > p_{\mathrm{lv}} \ \text{(open valve)} \\ 0, & \text{otherwise.} \end{cases}
\end{aligned}$$

(The expressions for q_{av} and q_{mv} are provided again for completeness.)

The pressures in each compartment are given by:

$$\begin{aligned}
p_{\mathrm{ao}} &= \frac{V_{\mathrm{ao}}}{C_{\mathrm{ao}}} \\
p_{\mathrm{sa}} &= \frac{V_{\mathrm{sa}}}{C_{\mathrm{sa}}} \\
p_{\mathrm{sv}} &= \frac{V_{\mathrm{sv}}}{C_{\mathrm{sv}}} \\
p_{\mathrm{vc}} &= \frac{V_{\mathrm{vc}}}{C_{\mathrm{vc}}} \\
p_{\mathrm{lv}} &= E_{\mathrm{lv}}(t)(V_{\mathrm{lv}} - V_{\mathrm{lv},0})
\end{aligned}$$

where variables C_i correspond to the compliance in compartment i (see Table 3 for nominal values) and $E_{\mathrm{lv}}(t)$ denotes the time-varying elastance described in Eq. (4).

References

1. Balsa-Canto E, Alonso AA, Banga JR (2010) An iterative identification procedure for dynamic modeling of biochemical networks. BMC Syst Biol 4:11
2. Beard DA, Mescam M (2012) Mechanisms of pressure-diuresis and pressure-natriuresis in Dahl salt-resistant and Dahl salt-sensitive rats. BMC Physiol 12:6
3. Boron W, Boulpaep E (2017) Textbook of medical physiology. Elsevier, Philadelphia
4. Brizzee BL, Russ RD, Walker BR (1991) Role of vasopressin in acutely altered baroreflex sensitivity during hemorrhage in rats. Am J Physiol 261:R677–R685
5. Bugenhagen SM, Cowley AW Jr, Beard DA (2010) Identifying physiological origins of baroreflex dysfunction in salt-sensitive hypertension in the Dahl SS rat. Physiol Genom 42:23–41
6. Chis O-T, Banga JR, Balsa-Canto E (2011) Structural identifiability of systems biology models: a critical comparison of methods. PLoS ONE 6:e27755
7. Cintrón-Arias A, Banks HT, Capaldi A, Lloyd AL (2009) A sensitivity matrix based methodology for inverse problem formulation. J Inverse Ill posed Prob 17:545–564
8. Cowley AW Jr (1992) Long-term control of arterial blood pressure. Physiol Rev 72:231–300
9. Di Rienzo M, Parati G, Radaelli A, Castiglioni P (2009) Baroreflex contribution to blood pressure and heart rate oscillations: time scales, time-variant characteristics and nonlinearities. Phil Trans R Soc A 367:1301–1318
10. Ellwein LM (2008) Cardiovascular and respiratory regulation, modeling and parameter estimation. PhD Thesis, Applied Math, NC State University, Raleigh, NC
11. Forsyth RP, Hoffbrand BI, Melmon KL (1970) Redistribution of cardiac output during hemorrhage in unanesthetized monkey. Circ Res 27:311–320
12. Gelman S (2008) Venous function and central venous pressure: a physiologic story. Anesthesiology 108:735–748
13. Greenway CV, Lautt WW (1986) Blood volume, the venous system, preload, and cardiac output. Can J Physiol Pharmacol 64:383–387
14. Hinojosa-Laborde C, Greene AS, Cowley AW (1988) Autoregulation of the systemic circulation in conscious rats. Hypertension 11:685–691
15. Johnson PC (1980) The myogenic response. In: Bohr DF, Somlyo AP, Sparks HV (eds) The handbook of physiology. The cardiovas-

cular system. Vascular smooth muscle. American Physiological Society, Bethesda, MD, Chapter 15, pp 409–442
16. Kapela A, Bezerianos A, Tsoukias NM (2008) A mathematical model of Ca2+ dynamics in rat mesenteric smooth muscle cell: agonist and NO stimulation. J Theor Biol 253:238–260
17. Kim T, Hendrich KS, Masamoto K, Kim SG (2007) Arterial versus total blood volume changes during neural activity-induced cerebral blood flow change: implication for BOLD fMRI. J Cereb Blood Flow Metab 27:1235–1247
18. Krames BB, Vanliere EJ (1966) Heart weight and ventricular weights of normal adult albino rats. Anat Rec 156:461–464
19. Leggett RW, Williams LR (1995) A proposed blood circulation model for reference man. Health Phys 69:187–201
20. Magder S, de Varennes B (1998) Clinical death and the measurement of stressed vascular volume. Crit Care Med 26:1061–1064
21. Marquis AD, Arnold A, Dean C, Carlson BE, Olufsen MS (2018) Practical identifiability and uncertainty quantification of a pulsatile cardiovascular model. Math Biosci. https://doi.org/10.1016/j.mbs.2018.07.001
22. Matzuka B, Mehlsen J, Tran H, Olufsen MS (2015) Using Kalman filtering to predict time-varying parameters in a model predicting baroreflex regulation during head-up tilt. IEEE Trans Biomed Eng 62:1992–2000
23. Miao H, Xia X, Perelson AS, Wu H (2011) On identifiability of nonlinear ODE models and applications in viral dynamics. SIAM Rev 53:3–39
24. Oosting J, StruijkerBoudier HAJ, Janssen BJA (1997) Validation of a continuous baroreceptor reflex sensitivity index calculated from spontaneous fluctuations of blood pressure and pulse interval in rats. J Hypertens 15:391–399
25. Ottesen JT, Mehlsen J, Olufsen MS (2014) Structural correlation method for model reduction and practical estimation of patient specific parameters illustrated on heart rate regulation. Math Biosci 257:50–59
26. Patterson SW, Piper H, Starling EH (1914) The regulation of the heart beat. J Physiol 48:465–513
27. Pope SR, Ellwein LM, Zapata CL, Novak V, Kelley CT, Olufsen MS (2009) Estimation and identification of parameters in a lumped cerebrovascular model. Math Biosci Eng 6:93–115
28. Raue A, Kreutz C, Maiwald T, Bachmann J, Schilling M, Klingmüller U, Timmer J (2009) Structural and practical identifiability analysis of partially observed dynamical models by exploiting the profile likelihood. Bioinformatics 25:1923–1929
29. Skrajnar S, Cerne M, Bozic M, Peternel L (2009) Effect of replacement fluids saline, gelofusine, and blood on biochemical and hematological parameters in rats subjected to repeated blood sampling. Med Sci Monit 15:BR293–BR300
30. Smith JJ, Forth CM, Erickson M (1994) Hemodynamic response to the upright posture. J Clin Pharmacol 34:375–386
31. Smith BW, Chase JG, Nokes RI, Shaw GM, Wake G (2004) Minimal haemodynamic system model including ventricular interaction and valve dynamics. Med Eng Phys 26:131–139
32. Transtrum MK, Machta BB, Sethna JP (2011) Geometry of nonlinear least squares with applications to sloppy models and optimization. Phys Rev E 83:036701
33. Trippodo NC (1981) Total circulatory capacity in the rat. Effects of epinephrine and vasopressin on compliance and unstressed volume. Circ Res 49:923–931
34. Williams ND, Wind-Willassen Ø, Wright AA, Program REU, Mehlsen J, Ottesen JT, Olufsen MS (2014) Patient-specific modelling of head-up tilt. Math Med Biol 31:365–392
35. Wu F, Yang F, Vinnakota KC, Beard DA (2007) Computer modeling of mitochondrial tricarboxylic acid cycle, oxidative phosphorylation, metabolite transport, and electrophysiology. J Biol Chem 282:24525–24537
36. Young DB (2010) Control of cardiac output. In: Granger DN, Granger JP (eds) Colloquium series on integrated systems physiology: from molecule to function to disease. Morgan and Claypool Life Sciences, San Rafael